8-2017

Development of Deep Site Specific and Reference Shear Wave Velocity Profiles in the Canterbury Plains, New Zealand

Michael Ryan Deschenes
University of Arkansas, Fayetteville

Development of Deep Site Specific and Reference Shear Wave Velocity Profiles in the Canterbury Plains, New Zealand

A thesis submitted in partial fulfillment
of the requirements for the degree of
Master of Science in Civil Engineering

by

Michael Ryan Deschenes
University of Arkansas
Bachelor of Science in Civil Engineering, 2015

August 2017
University of Arkansas

This thesis is approved for recommendation to the Graduate Council.

Dr. Clinton M. Wood
Thesis Director

Dr. Michelle L. Bernhardt
Committee Member

Dr. Gary S. Prinz
Committee Member

ABSTRACT

Deep (typically >1000 m) shear wave velocity profiles were developed across the Canterbury basin at nine strong motion stations using a combination of active and passive surface wave methods and horizontal to vertical spectral ratio measurements. A multi-mode, multi-method joint inversion process, which included Rayleigh and Love wave dispersion and horizontal to vertical spectral ratio data, was used to estimate the shear wave velocity profiles at each site. A-priori geologic information was utilized in defining preliminary constraints on the complex geologic layering of the Canterbury basin. At sites where interbedded layers were present, velocity reversals were considered in the inversion. Shear wave velocity profiles developed as part of this study were combined with the median profiles from 14 Christchurch sites detailed in a separate study, to develop a suite of region and soil specific reference shear wave velocity profiles for the Canterbury basin. Site specific and reference shear wave velocity profiles developed as part of this study can be used for back-analysis of earthquake ground motions, forward analysis of future ground motions, full 3D physics based simulations, or to refine 3D velocity models for the region.

TABLE OF CONTENTS

1. INTRODUCTION

The 2010 and 2011 Canterbury earthquake sequence (CES) occurred on a system of previously unknown faults within kilometers of and underneath the city of Christchurch, New Zealand (Barnes et al. 2011). The most damaging of these earthquakes was the February 22, 2011 moment magnitude 6.2 event, which occurred underneath the city. This was the costliest earthquake in New Zealand's history with 185 fatalities and extensive structural damage and collapse. Approximately, half the buildings in the central business district (CBD) had to be demolished for economic and/or safety reasons (Taylor et al. 2011). Liquefaction was a major factor in damage to structures in the CBD (Cubrinovski et al. 2011, Green et al. 2012). Furthermore, extensive liquefaction and lateral spreading in the suburbs surrounding Christchurch caused severe damage to nearly 15,000 homes with over half of these being deemed beyond economical repair (Cubrinovski et al. 2011, Green et al. 2012).

Ground motions from the CES were recorded by a dense network of strong motion stations (SMS) located in the city of Christchurch and the greater Canterbury region. These ground motions were quite complex in some areas with combined stratigraphy, basin, and directivity effects (Cubrinovski et al. 2011). Specifically, long-period motions were amplified and ground shaking durations were lengthened as a result of surface waves generated by seismic waves traveling through the Canterbury basin (Cubrinovski et al. 2011). To develop proper site effects estimates and ground motion predictions, the shallow and deep seismic velocity structure of the region must be known. However, prior to the CES very little information was available regarding the shear wave velocity (V_s) structure of the Canterbury region beyond a depth of 30 m.

Following the CES, researchers began charactering the shallow and eventually deep dynamic structure of the region. Surface wave measurements were made by Wood et al. (2011) and

Wotherspoon et al. (2014) to characterize the near surface (top 30 m) at SMS located throughout Christchurch. Following the shallow characterization efforts, surface wave testing and horizontal-to-vertical spectral ratio (HVSR) measurements were made in the urban Christchurch area to develop deep V_s profiles to bedrock (Wood et al. 2014, Teague et at. 2015, Teague et al. 2017). Although the exact testing locations for the deep Vs profiles did not correspond to the specific location of SMS due to site access limitations, the profiles can be used with site specific shallow V_s information by Wood et al. (2011) and Wotherspoon et al. (2014) to develop site specific V_s profiles to bedrock at these SMS. Extensive HVSR measurements were carried out by Wotherspoon et al. (2015) at 80 sites across the Canterbury plains (including Christchurch). Using this and many other sources, a 3D seismic velocity model for the Canterbury basin (referred to as the CVM throughout the remainder of the paper) was developed by Lee et al. (2015) and Lee et al. (2017) which defines the depth of geologic unit boundaries for all major geologic units in the Canterbury region. Although a significant amount of Vs information is now available for the Canterbury region, much of it focuses on the city of Christchurch leaving many SMS and a significant portion of the Canterbury basin uncharacterized.

This paper details efforts to characterize the deep (typically >1000 m) V_s structure of the Canterbury basin and to create a suite of region specific reference V_s profiles for the Canterbury basin. Both active and passive source Rayleigh and Love type surface wave data were collected along with HVSR measurements at nine SMS in the Canterbury plains. V_s profiles were inverted from the surface wave data and HVSR measurements using a multi-mode, multi-method joint inversion process. The resulting V_s profiles were combined with the median V_s profiles from the 14 Christchurch sites detailed in Teague et al. (2017) to develop a suite of region and soil specific reference V_s profiles for the Canterbury Basin.

2. CANTERBURY GEOLOGY

The Canterbury basin is located on the central-eastern portion of the South Island of New Zealand. It extends from the east coast approximately 20-30 km to the Southern Alps mountain range. The city of Christchurch is set on the eastern edge of the basin along Pegasus Bay. The city is bordered by the Banks Peninsula Volcano to its southeast and the coast of Pegasus Bay to the east. The Canterbury basin is composed of alluvial and pluvial layers consisting of dense layers of gravel along the western edge and transitioning into interbedded layers of gravel and softer deposits near the eastern coast. Shown in Figure 1 are the transition between entirely gravel layers into layers of interbedded gravel and softer materials along with the change in elevation towards the coastline (Figure 1a) and the interbedded layering at Bexley Well 2 (Figure 1b). The softer interbedded layers are typically encountered in the first 250 m and are part of the Quaternary geologic unit. The top of the Quaternary unit is composed of the Christchurch or Springston formations. The Christchurch formation is typically encountered nearer to the coast and consists of mixed gravel, sand, silt, clay, and peat deposits, whereas the Springston formation is typically encountered further inland and primarily composed of alluvial sands and gravels (Lee et al. 2015 and Teague et al. 2017). As presented in Figure 1a, the Springston formation is underlain by several thick gravel formations. Whereas, the Christchurch Formation is underlain by interbedded layers of gravel and softer deposits of mixed sand, silt, clay, and peat. The alternating soft and stiff layers under the Christchurch Formation produce numerous large velocity contrasts, which can significantly affect seismic wave propagation leading to basin effects and nonlinear soil behavior (Lee et al. 2015). Underlying the potentially interbedded quaternary layers are the Pliocene (Kowai), Miocene, and Paleogene gravel formations located above the Torlesse Terrane rock formation (Barnes et al. 2016). Although not present at the

Bexley Well 2 (Figure 1b), there is a shallow layer of volcanic material from the Banks Peninsula Volcano overlying the Miocene and Paleogene formations, and interjecting between the Pliocene and Miocene units. The volcanics have velocities slightly lower than the basement material, but significantly greater than the surrounding gravel layers. The Banks Peninsula volcanics are typically encountered at depths ranging from approximately 350 to 700 m in the southeastern portion Christchurch with the depth to volcanics increasing with distance from the Banks Peninsula (Barnes et al. 2016, Lee et al. 2015). Therefore, near the Banks Peninsula a shallow rock artifact relative to the basement depth is anticipated. The bedrock depth in the other portions of the basin can vary greatly with some locations over 2000 m below the surface (Lee et al. 2015).

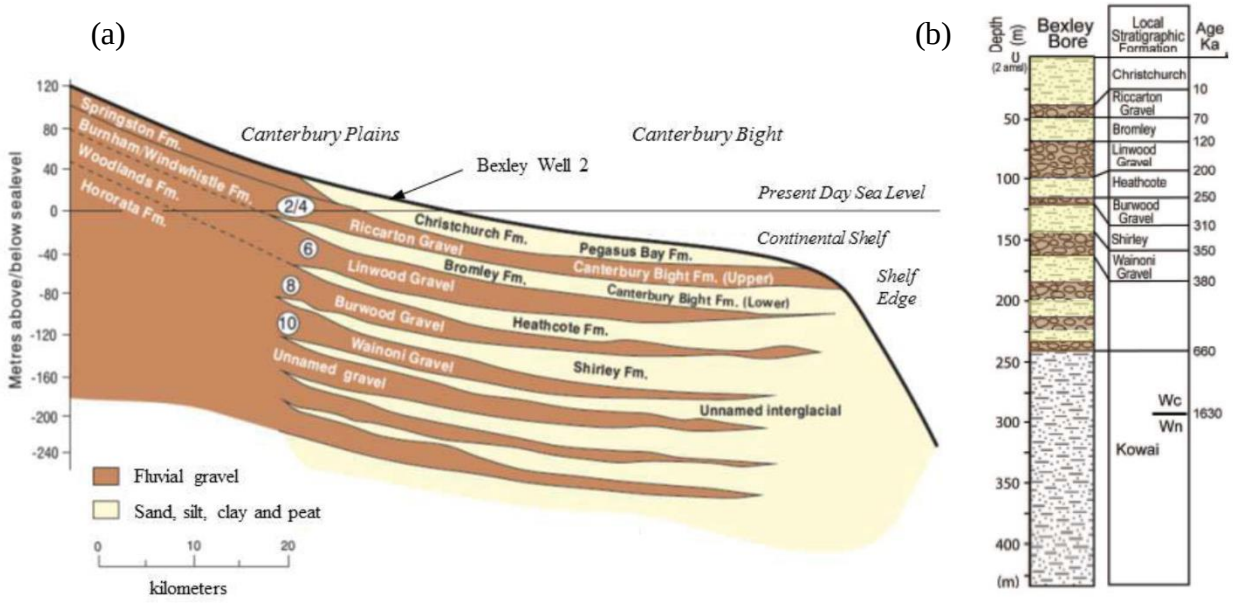

Figure 1. (a) Geology beneath Christchurch and Pegasus Bay showing a sequence of deep interlayered gravel and sand formations, and (b) simplified representation of the geologic layering from Bexley Well 2 (modified from Forsyth et al. 2008, Barnes et al. 2011 and Teague et. al 2017).

3. SITE LOCATIONS AND TESTING METHODOLOGY

Surface wave and HVSR measurements were conducted at nine SMS within the Canterbury Basin (see Table 1). The location of each station is illustrated in Figure 2 along with the location of the 14 Christchurch sites where deep Vs profiles were developed by Teague et al. (2017). Five of the sites tested in this study are located along the western portion of the basin where only gravel layers are present in the subsurface, whereas, four stations are located near the coastline where interbedded soft layers are present.

Table 1. Canterbury strong motion stations where surface wave and HVSR measurements were conducted.

Site Name	Code	Latitude	Longitude	V_{S30} (m/s)	Site Condition
Darfield High School	DFHS	-43.489666	172.102158	518	Gravel only
Greendale	GDLC	-43.586175	172.088746	457	Gravel only
Hororata School	HORC	-43.539633	171.959897	531	Gravel only
Lincoln C&F Research	LINC	-43.623175	172.468000	292	Interbedded
Rakaia School	RKAC	-43.751452	172.023135	452	Gravel only
Rolleston School	ROLC	-43.592814	172.381093	447	Interbedded
Selwyn Lake Road	SLRC	-43.675130	172.317520	327	Interbedded
Swannanoa School	SWNC	-43.369422	172.495356	546	Gravel only
Templeton School	TPLC	-43.549989	172.471954	398	Interbedded

Surface wave measurements were made at each SMS using a combination of active-source Multi-channel analysis of surface waves (MASW) and passive-source microtremor array measurements (MAM). A general layout of the different tests performed at each station is provided in Figure 3a. The MASW method was used to collect both Rayleigh and Love type active surface wave data at each SMS (Park 1999). MASW testing was conducted using an array of 24 or 48, 4.5 Hz vertical (Rayleigh) or horizontal (Love) geophones with a uniform space of 2 m between each geophone (array length of 46 or 94 m, respectively) as shown in Figure 3b. Rayleigh and Love waves were generated using vertical or horizontal blows from a 5.4 kg sledgehammer, respectively. To produce high quality data, allow for uncertainty quantification,

and to minimize nearfield effects, multiple source offsets of 5, 10, 20, and 40 m from the first geophone in the array were utilized. A total of 10 sledgehammer blows were stacked at each source location to improve the signal-to-noise ratio of the recorded waveforms.

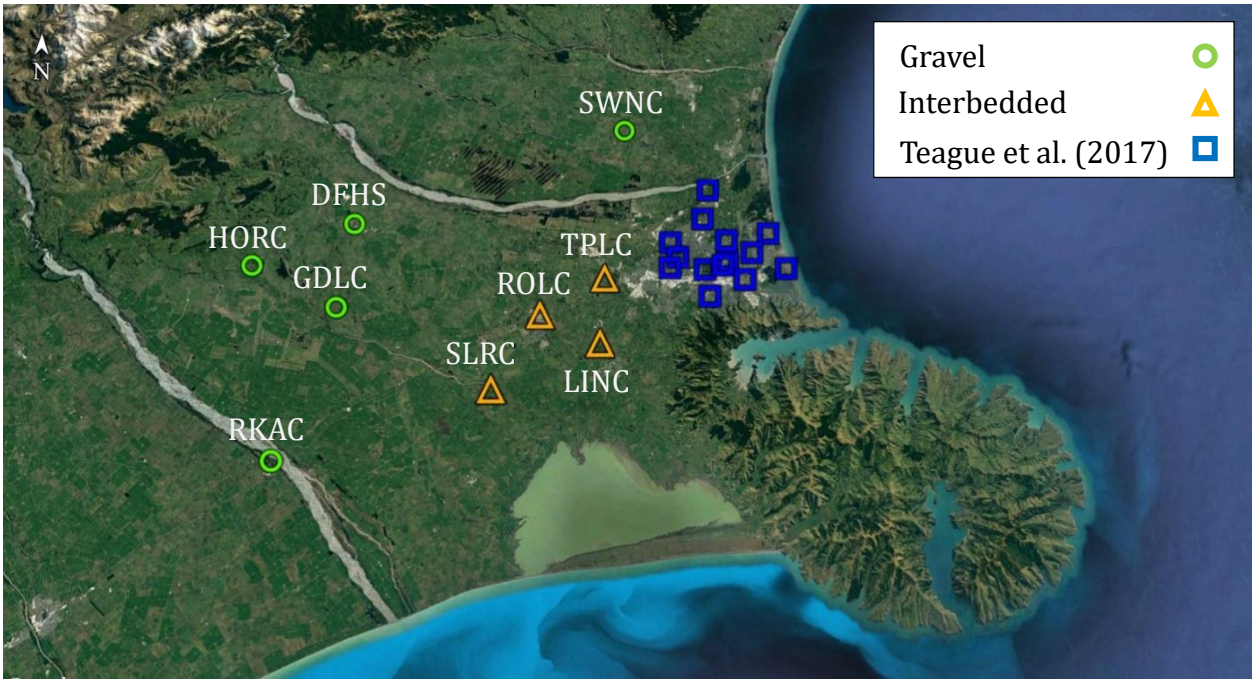

Figure 2. Locations of the nine SMS where surface wave and HVSR measurements were conducted as part of this study and 14 locations characterized by Teague et al. 2017. SMS testing locations are color coded based on the site geology.

MAM measurements were made using circular arrays of ten three-component trillium compact, 20 second (0.05 Hz) broadband seismometers (Figure 3c). These seismometers were generally arranged with one seismometer at the center and nine uniformly distributed around the circumference. However, at some sites deviations were made due to site constraints. At every site, array diameters of 50, 200, and 500 m were used with a 1000 m diameter array used at select locations. Ambient noise was recorded for one hour for the 50 m and 200 m arrays and two hours for the 500 m and 1000 m arrays. A typical installation of the trillium compact seismometer is presented in Figure 3c.

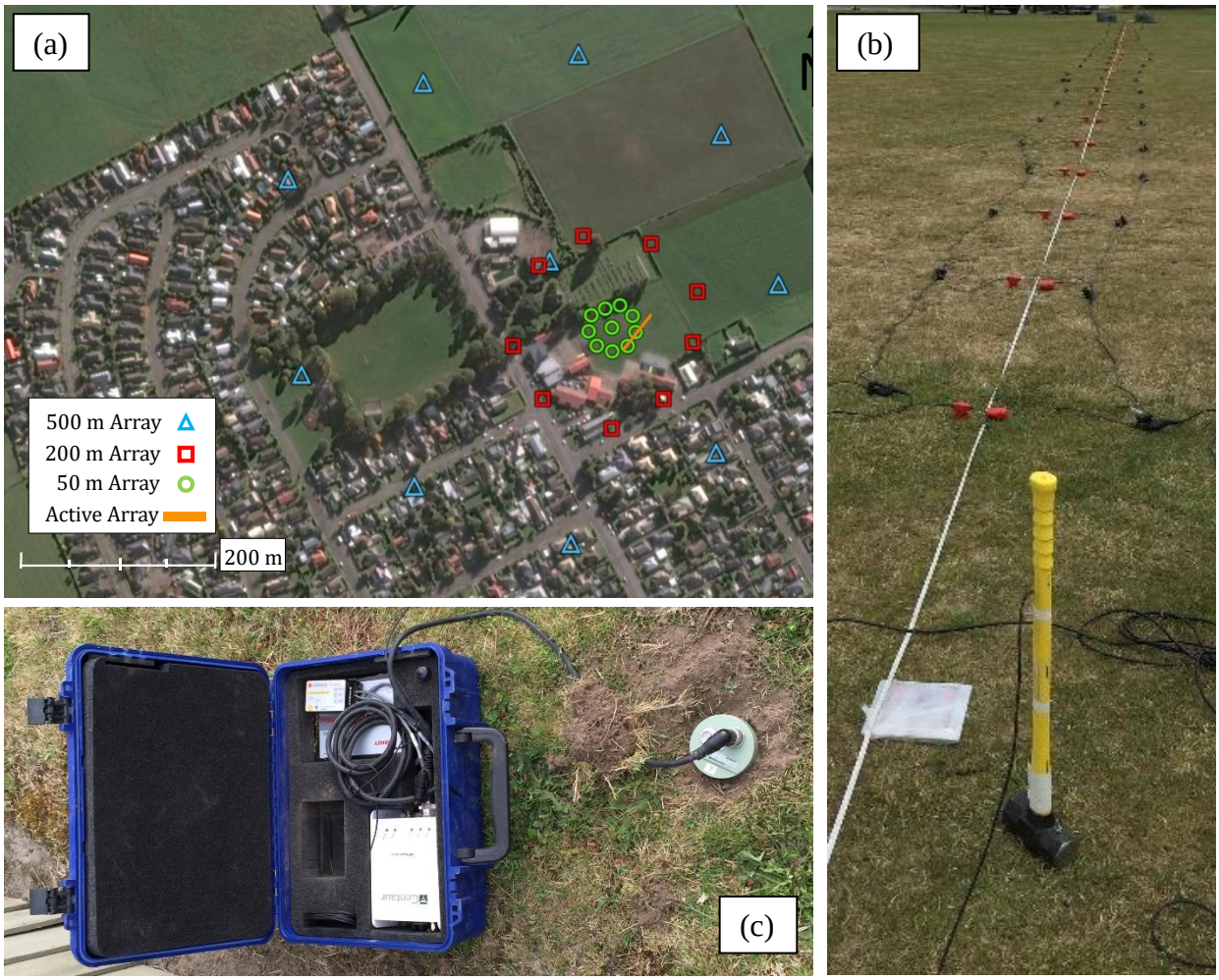

Figure 3. Typical testing configuration at each of the nine SMS for (a) the circular arrays (50 m, 200 m, 500 m, and where applicable 1000 m) used to record passive microtremors (MAM) and the linear active-source (MASW) arrays, (b) the active-source linear array of 4.5 Hz geophones with horizontal (Love wave) geophones on the right of the measuring tape and vertical (Rayleigh wave) geophones on the left, and (c) a trillium compact broadband seismometer used in the passive MAM array.

4. DATA PROCESSING

4.1. DISPERSION PROCESSING

The active-source MASW data were processed using the Frequency Domain Beamformer (FDBF) method in combination with the multiple-source offset technique (Zywicki 1999, Cox and Wood 2011). The use of multiple source offsets during data collection and processing allows for quantifying dispersion uncertainty and identification of near field contamination. For each

source offset (5, 10, 20, 40 m), both Rayleigh and Love wave dispersion data were developed from the vertical and horizontal velocity records, respectively. The dispersion data from each source offset were combined to form a single composite experimental dispersion curve and all identifiable near-field and effective mode data were eliminated. The remaining composite dispersion curve was divided into 50 frequency bins distributed on a logarithmic scale between 1 and 100 Hz. The mean phase velocity and standard deviation were computed for each bin and carried through to the inversion process.

Rayleigh and Love wave dispersion data were computed using the HRFK method (Capon 1969) from ambient (MAM) noise recorded using each of the circular arrays from the vertical and horizontal components of the seismometers, respectively. The time records for each array were divided into 180 second time windows resulting in 20 to 40 windows for each array ensuring a sufficient number of cycles for each frequency. Peak wavenumber pairs were selected at 125 frequency points distributed logarithmically between 0.1 and 20 Hz for each time window resulting in 20 and 40 phase velocity values for each frequency. A single composite experimental dispersion curve was then developed based on the individual dispersion curves for each array. To develop Love wave dispersion data, the horizontal components are rotated to align one horizontal component of the sensor with the azimuth of the Rayleigh wave propagation for each frequency, which was determined during the Rayleigh wave analysis (i.e., using the vertical components). The component perpendicular to Rayleigh wave propagation is assumed to be in line with the direction of maximum Love wave particle motion. However, this presumes Love waves arrive from the same azimuth as the Rayleigh waves, which may not always be the case. Therefore, caution should be used when analyzing Love waves from 2D passive arrays to ensure true Love wave propagation was measured in the field. In this study, Love wave dispersion data was

compared to Rayleigh wave dispersion data from the HRFK and MSPAC processes and inversions conducted with and without Love wave dispersion data were compared to ensure the Love wave dispersion data are consistent with Love wave propagation.

The MSPAC method (Bettig el al. 2001) was also used to compute Rayleigh wave dispersion data from the passive-source MAM data. Sensor pairs were divided into five circular sub-array rings. An average autocorrelation value was computed for each ring, which enables processing of imperfect circles (Bettig et al. 2001). Auto-correlations were developed by dividing the time records into 180 second windows and computing auto-correlation values at 125 frequency bins spaced between 0.1 and 10 Hz logarithmically. Average and lower- and upper-bound phase velocities were selected from histograms. These were used to define dispersion curves for each array with associated uncertainty. The dispersion curves from each array were combined to form a single composite experimental dispersion curve.

To create a mix-method composite dispersion curve, the individual curves from each array and method were first cleared of any outlying phase velocity points. The dispersion curves from each array were then compared to identify significant deviations from the composite trend. Examples of such deviations are effective mode data and near-field effects. These deviations were removed from the dispersion data. Dispersion data from the HRFK method with wavenumber outside of the maximum and minimum array resolution limits ($k_{min}/2$ and $k_{max}/2$ per Wathelet et al. 2008) were considered less reliable then data within the limits and removed in most cases. However, some of this data was preserved if it compared well with data from other arrays or with dispersion data from other methods, (i.e, MSPAC and MASW). Therefore, some dispersion data beyond the array resolution limit were included in the inversion. Following

elimination of poor quality data, the dispersion curves from all arrays were averaged to form a single composite dispersion curve.

4.2. HVSR PROCESSING

The passive-source (MAM) array data were also used to develop HVSRs for each of the ten seismometers for all arrays. Time records were divided into 180 second windows with an HVSR curve computed for each window. The squared average of the horizontal components were used for spectral calculations. Konno and Ohmachi (1998) frequency smoothing, with a coefficient of 40, was used to reduce spikes in the Fourier amplitude spectra. A single average HVSR peak, with associated standard deviation, was computed from the HVSR peaks of all sensors in all arrays (30 to 40 peaks) if the peaks were consistent between sensors and arrays (i.e., 1D subsurface structure). The fundamental HVSR peak was assumed equal to the fundamental Rayleigh wave ellipicity peak and used in a joint inversion with the dispersion data to constrain the depth to bedrock (Scherbaum et al. 2003, Arai and Tokimatsu 2005, Parolai et al. 2005, Piccozi et al. 2005, Rosenblad and Geotz 2010).

4.3. INVERSION

The composite experimental dispersion curve and HVSR peak for each site were used in a joint inversion using the Geopsy software package Dinver (Wathelet et al. 2008). Dinver operates by generating trial V_s profiles using a neighborhood algorithm (Thomson 1950, Haskell 1953, Dunkin 1965, Knopoff 1964) within user-defined constraints. A corresponding theoretical dispersion curve is computed for each V_s profile and compared with the experimental dispersion curve to estimate the goodness of fit using a misfit function. The user defined constraints or layer parameterization for the inversion are velocity (V_s and V_p), depth, Poisson's ratio, density, and

the number of layers in the soil profile. The use of a parameterization in Dinver aids the inversion process by reducing the size of the solution space from which velocity profiles can be generated. However, the accuracy of the V_s profiles obtained from the inversion have been shown to be greatly dependent on the parameterization used in the inversion (DiGiulio et al. 2012). Therefore, it was an essential component of the inversion processes to properly arrange the parameterization for each site.

The layer parameterization at each site was developed based on estimations of the regional geology primarily detailed in Lee et al. (2017). Water and petroleum well logs along with seismic reflection, shallow (30 m) surface wave testing, and CPT tests for V_s correlations conducted over the Canterbury region were compiled in generating a velocity model for the Canterbury region (Lee et al. 2017). Using the geologic model, an approximation of the soil strata down to bedrock were developed for each SMS location. Seismic reflection data allowed for more detailed estimation of layer interfaces; however, the accuracy of the velocity values from reflection are negatively influenced by the previous discussed velocity inversions in the subsurface. Therefore, the reflection data from the velocity model was primarily used as a constraint on the range of depth and thickness for each layer in the parameterization rather than velocity limits for layers. A range of velocity, density, and Poisson's ratio values for each layer were estimated based on the type of material expected in each geologic strata. The range of V_s values was defined based on V_s reference curves, by Lin et al. (2014), which are dependent on soil type and mean effective confining pressure. Poisson's ratio was allowed to vary between 0.25-0.35 for soils above the water table. Poisson's ratio for soils below the water table was based on a V_p of 1500 m/s, however, at depths where V_s was greater than 750 m/s, V_p was

allowed to increase beyond 1500 m/s to keep Poisson's ratio between 0.25-0.35. A uniform density of 2000 kg/m^3 was used for soils and 2300 kg/m^3 for basement rock.

For each site, 1-2 million models with corresponding Vs profiles, Rayleigh and Love wave dispersion curves, and ellipicity curves were generated in an effort to obtain the best dispersion curve fit. Within Dinver, the misfit or the overall 'closeness' between the experimental and theoretical dispersion curve is computed for each model. In order to obtain the closest fit of the experimental dispersion curve, Dinver attempts to minimize the misfit at each frequency point along the experimental dispersion curve. The misfit is computed following a modification of the Wathelet (2004) misfit equation to account for both the HVSR peak and the dispersion curve with associated uncertainty as detailed in Teague et al. (2017). Misfit values less than one indicate that the theoretical dispersion curve and ellipicity peak primarily fit within one standard deviation of the experimental dispersion curve and ellipicity peak. A misfit value greater than one, indicates that the theoretical dispersion curve does not adequately represent the experimental data. However, misfit values can vary greatly between various locations (Cox and Teague 2016) dependent of the quality and quantity of dispersion data and the complexity of the geology (Teague et al. 2017). Typically, the 1000 lowest misfit or closest fit profiles were utilized as a representative sample to generate a characteristic median V_s profile and to determine uncertainty for each site.

5. SURFACE WAVE INVERSION RESULTS

The results for the Templeton (TPLC) site will be discussed in detail as a specific example of the challenges in the inversion process, before the results for all sites are presented.

5.1. TEMPLETON (TPLC) RESULTS

The TPLC SMS is located in the small town of Templeton on the outskirts of Christchurch and near the coast where interbedded soft and stiffer soil layers are present in the first 150 m. Therefore, velocity reversals were expected in the first 150 m, requiring a more complex inversion to account for velocity reversals instead of a simpler normally dispersive inversion. Figure 4 contains the Rayleigh (Figure 4a) and Love (Figure 4b) wave dispersion data from the TPLC site. Fundamental mode Rayleigh wave dispersion data (R0) was resolved between 10 and 50 Hz with the MASW and HRFK data overlapping well. Between 1 and 10 Hz a complex area of wave propagation was observed with the HRFK resolving a higher (R1) or effective mode and the MSPAC resolving a lower (R0) or effective mode. A majority of the data in this region was excluded from the inversion due to effective mode propagation. The Rayleigh wave data between 0.1 and 1 Hz were considered fundamental mode or first higher mode (R0-R1) data. Typically, at low frequencies (<0.5 Hz), the MSPAC results indicated a lower dispersion velocity than the HRFK results. As noted by Asten and Boore (2005), low frequency HRFK data can trend toward higher dispersion velocities than MSPAC data due to azimuthal smearing when waves are impinging on the array from multiple azimuthal directions. However, HRFK data is often more reliable when waves propagate from single azimuthal direction. Therefore, for each analysis either MSPAC or HRFK data was removed from portions of the frequency range with the HRFK often trusted at higher frequencies and MSPAC data trusted at low frequencies. For the Love wave dispersion curve, the first higher mode (L1) was resolved over the entire frequency range.

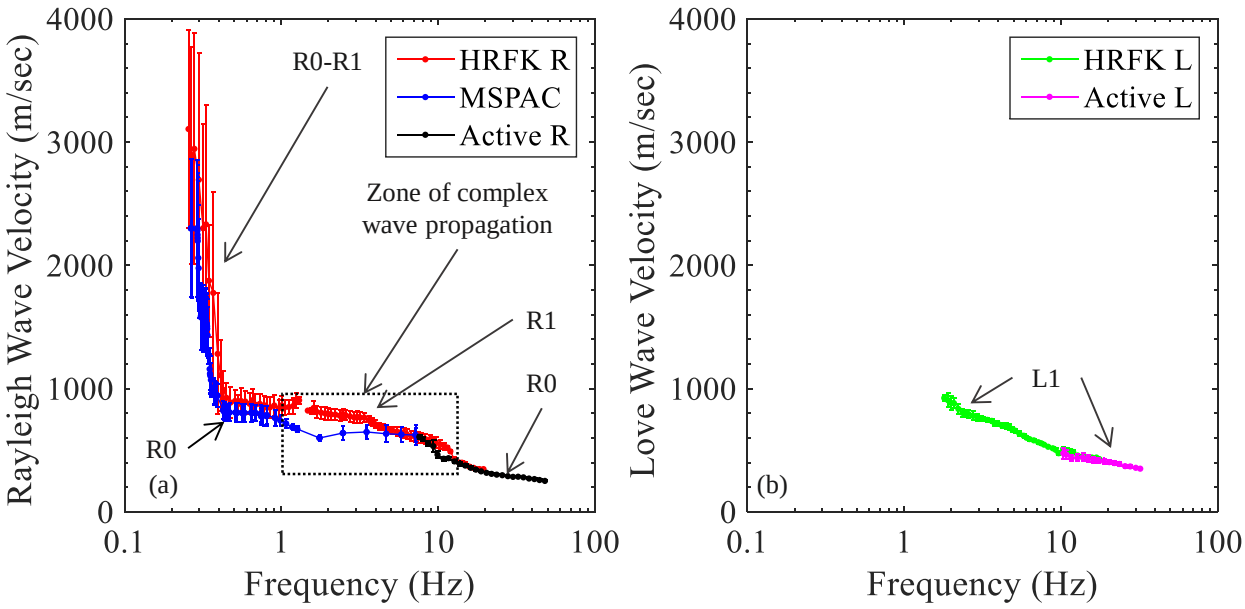

Figure 4. Combined dispersion data from the active- and passive-source surface wave methods. Mode and regions of transition are denoted by arrows for (a) Rayleigh wave active MASW, passive HRFK, and passive MSPAC, and (b) Love wave active MASW and passive HRFK data.

The Rayleigh and Love wave theoretical dispersion curves for the 1000 lowest misfit velocity models for the TPLC site are presented along with the experimental dispersion data in Figure 5a and 5b, respectively. The theoretical dispersion curves associated with the median Vs profile from the 1000 lowest misfit Vs profiles are also included. The theoretical dispersion curves fit the fundamental and first higher mode experimental data well with a minimum misfit value of 0.39. Due to the transition between modes, some of this portion of the curve was removed prior to the final inversion. Effective or higher mode data, which is mistakenly classified as fundamental mode, will potentially have much higher V_s than what is representative of the subsurface. Through numerous iterations, the sections of the data determined to be effective mode were not used in the solution. Therefore, the theoretical curves do not closely match that portion of the experimental curve.

The experimental HVSR curve with associated plus- and minus-one standard deviation is provided in Figure 5c. The average HVSR peak measured at the TPLC site was 0.179 ± 0.02 Hz represented by the vertical dashed black line in Figure 5c. The fundamental mode Rayleigh wave ellipicity curve, calculated from the median V_s profile of the top 1000 lowest misfit V_s profiles was calculated to be 0.192 Hz, which is within the standard deviation of the experimental peak.

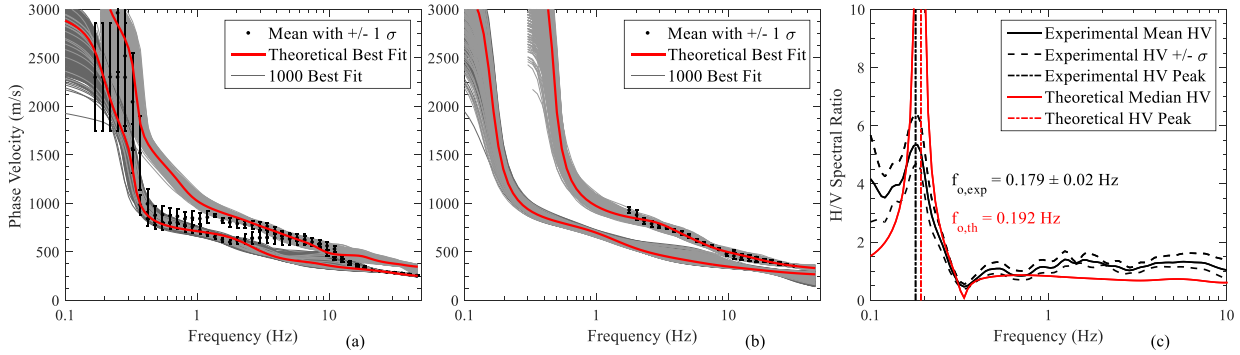

Figure 5. Experimental dispersion data and theoretical fits for the 1000 lowest misfit V_s profiles at the TPLC site, (a) Rayleigh wave and (b) Love wave. (c) Experimental HVSR curve and theoretical HVSR curve for the median of the 1000 lowest misfit V_s profiles at the TPLC site.

The 1000 lowest misfit V_s profiles and the standard deviation in the natural logarithm of the V_s profiles (sigma ln V_s) associated with the profiles (sigma ln Vs or $\sigma_{(\ln(Vs)}$ approximates coefficient of variation for log normal distribution), for the TPLC site are shown in Figure 6a with geologic layering for the top 200 m and in Figure 6b for the top 2000 m. In the first 150 m of the profile, there are several major velocity reversals, which correspond to distinct geologic units determined from the CVM. Although layering from the CVM was used to define the parameterization. The inversion algorithm was allowed some freedom to determine the most accurate layering for the experimental data. Therefore, the derived V_s profiles may vary slightly from the layering provided by the CVM. Even though these velocity reversals are beyond the blind resolution ability of methods used, their use in the inversion process provides a better

representation of the geology of the site than a simplified normally dispersive model (Wood et al. 2014, Teague et al. 2017).

To ensure reasonable velocities, V_s profiles from the inversion were compared to soil specific reference V_s profiles (Lin et al. 2014) as shown in Figure 6a. The Lin et al. (2014) reference V_s profiles are used to provide general estimates of V_s as a function of soil type and mean confining stress. Overall, the developed V_s profiles seems to match well with the dense gravel and fine dense gravel curves in regions identified as gravels by the CVM. For layers identified as sand by the CVM (i.e., 30 m, 90 m and 130 m), the velocities match well with the sand reference curves especially for the two shallow sand layers. However, for the third sand layer at 130 m, the velocity of the median V_s profile matches closer with the dense gravel curve. This is still considered reasonable given the reference V_s profiles were based largely on data from the top 30-60 m. Beyond 150 m, the velocity gradually increases with depth as the soil structure is made up of thick geologic units of gravel (Pliocene, Miocene, and Paleogene) down to bedrock. Bedrock depth in the CVM at TPLC was 1244 m; however, bedrock depth for the 1000 lowest misfit V_s profiles varied from 1260 to 1800 m with the bedrock V_s ranging from 2465 m/s to 3633 m/s (median depth and V_s of 1634 m and 3224 m/s, respectively). This large variation in the V_s profiles indicates the bedrock depth and bedrock velocity are poorly constrained by the inversion process. However, the measured HVSR peak of 0.179 Hz suggests bedrock may be deeper than the median depth of 1634 m, since the theoretical ellipicity peak of the median V_s profile was 0.192 Hz. An HVSR peak corresponding to the bedrock depth provided by the CVM (i.e., 1244 m) would require a much higher frequency than the experimental and theoretical peaks for the TPLC site. Trial inversions with shallower bedrock depths did not yield acceptable dispersion

fits nor ellipicity peaks of comparable frequency to the measured HVSR curve. Therefore, the bedrock depth is likely deeper than that provided by the CVM.

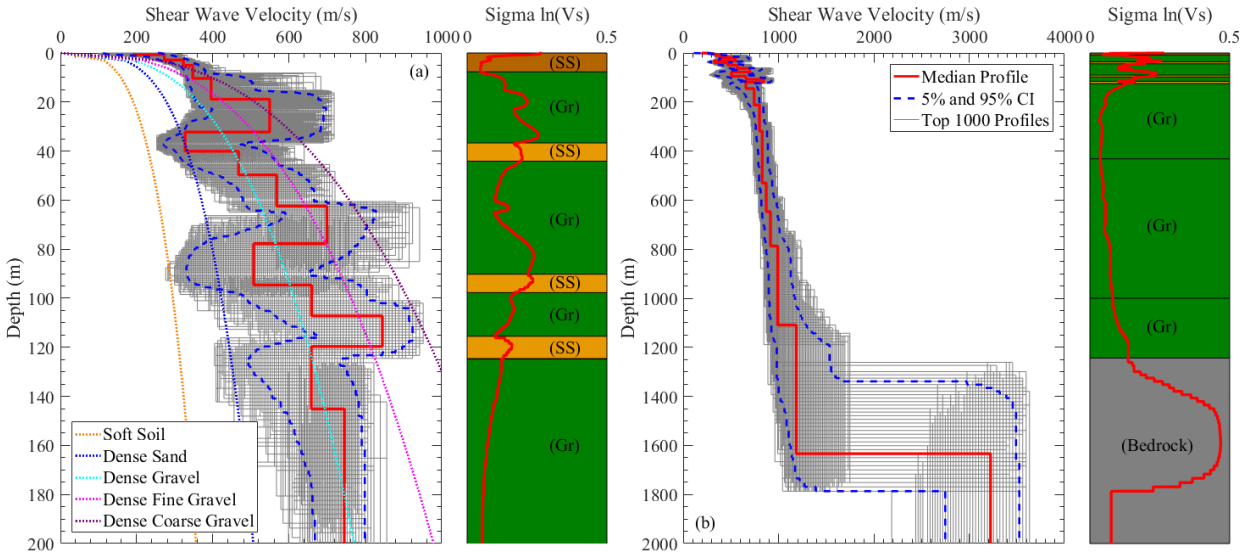

Figure 6. Shear wave velocity profiles resulting from the inversion for the Templeton SMS location with the $\sigma_{(\ln(Vs)}$ to show uncertainty along with geologic layering at the site for (a) the top 200 m and (b) the top 2000 m. The shear wave velocity profiles from 1000 lowest misfit inversion models are provided in gray with the median of all 1000 profiles in red. The blue dashed lines represent the counted 5 and 95 percent confidence intervals of the data. Gr = gravel and SS = soft soil.

5.2. Results from All Sites

The Rayleigh and Love wave theoretical and experimental dispersion data from the inversions for all nine SMS locations are shown in Figure 7. The theoretical dispersion curves in Figure 7 include the 1000 lowest misfit dispersion curves and median dispersion curve calculated from the median of the 1000 lowest misfit V_s profiles. Although the TPLC inversion included only fundamental and first higher mode data, inversions at most other sites include fundamental, first higher, second higher, and effective mode data. Similar to the TPLC site most sites tested tended to have fundamental mode Rayleigh wave propagation at frequencies greater than 10 Hz and less than 1 Hz. Higher or effective mode Rayleigh wave behavior tended to dominate within

a zone of complex wave propagation (see Figure 4a) typically between 1 and 10-20 Hz for most sites. Also, similar to TPLC, Love waves tended to propagate at the first higher mode for most sites with some sites having fundamental mode Love wave propagation at frequencies higher than 10-20 Hz. At each site, a misfit of less than 0.80 was achieved with the theoretical curves fitting the experimental data well for modes that were well defined (i.e., not effective modes).

Horizontal-to-vertical spectral ratios results from all sites are shown in Figure 8. The experimental mean HVSR curve with associated plus- and minus one standard deviation bounds and the peak spectral ratio are provided for each site. Experimental HVSR peaks ranged from 0.148 Hz to 0.196 Hz corresponding to the bedrock depth and soil stiffness for each site. However, the experimental peak from SWNC did not meet the criteria for a clear peak per SESAME (2004) and may not be representative of bedrock depth. Present at several sites (DFHS, GDLC, RKAC, ROLC, SLRC, and LINC) were slight minor peaks between 0.7 to 1.2 Hz, typically, the frequency of these peaks corresponded to the depth of the Riccarton or Linwood gravel formations. The theoretical median HVSR curve and peak for each site are included in Figure 8. Theoretical peaks ranged from 0.140 Hz to 0.201 Hz and were typically within 0.004 to 0.020 Hz ($< \pm 1\sigma$) of the experimental average peaks.

Figure 9 contains the top 1000 V_s profiles, the lowest misfit profile, the median of all 1000 lowest misfit profiles, and the counted 5 and 95 percent confidence intervals of the V_s data from the inversion for each site. Also shown is the sigma ln V_s in the plot adjacent to each V_s profile. The median V_s profiles for each site are also tabulated in Table 2. The ROLC, SLRC, and LINC sites, like the TPLC site are located on interbedded deposits closer to the east coast. The remaining five sites are located on gravel only deposits closer to the Southern Alps. As with the

TPLC V_s profiles, sites with interbedded deposits have a higher sigma ln V_s in the top 150 m, while gravel only sites typically have a lower sigma ln Vs in that range. Also, similar to TPLC,

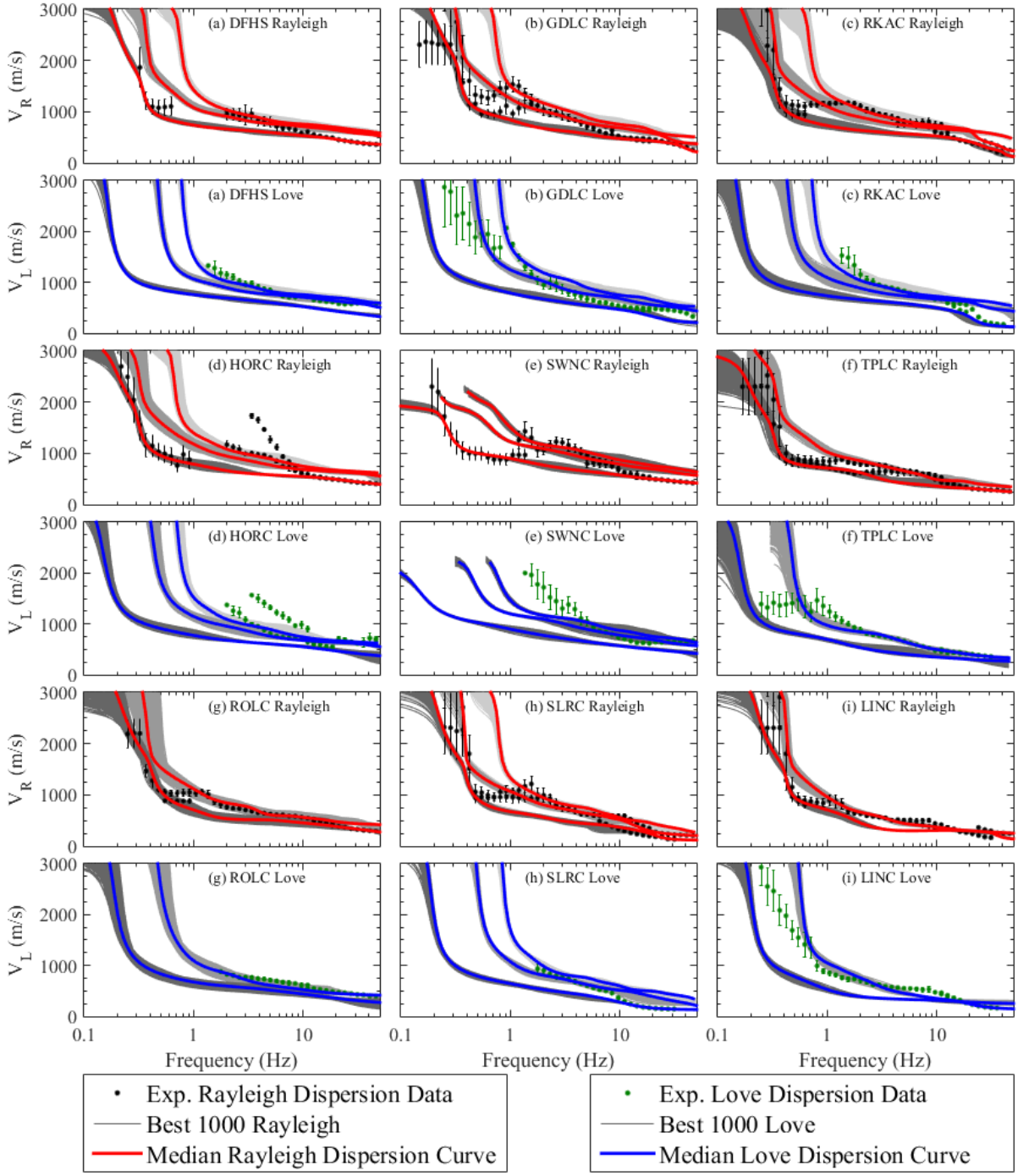

Figure 7. Rayleigh and Love wave dispersion data from all nine Canterbury sites, including raw experimental dispersion targets with the dispersion curve generated from the median velocity profile (the median dispersion curve) overlaying the 1000 best or lowest misfit models for each

applicable mode. A median and 1000 lowest misfit fit theoretical dispersion curves are provided for each mode.

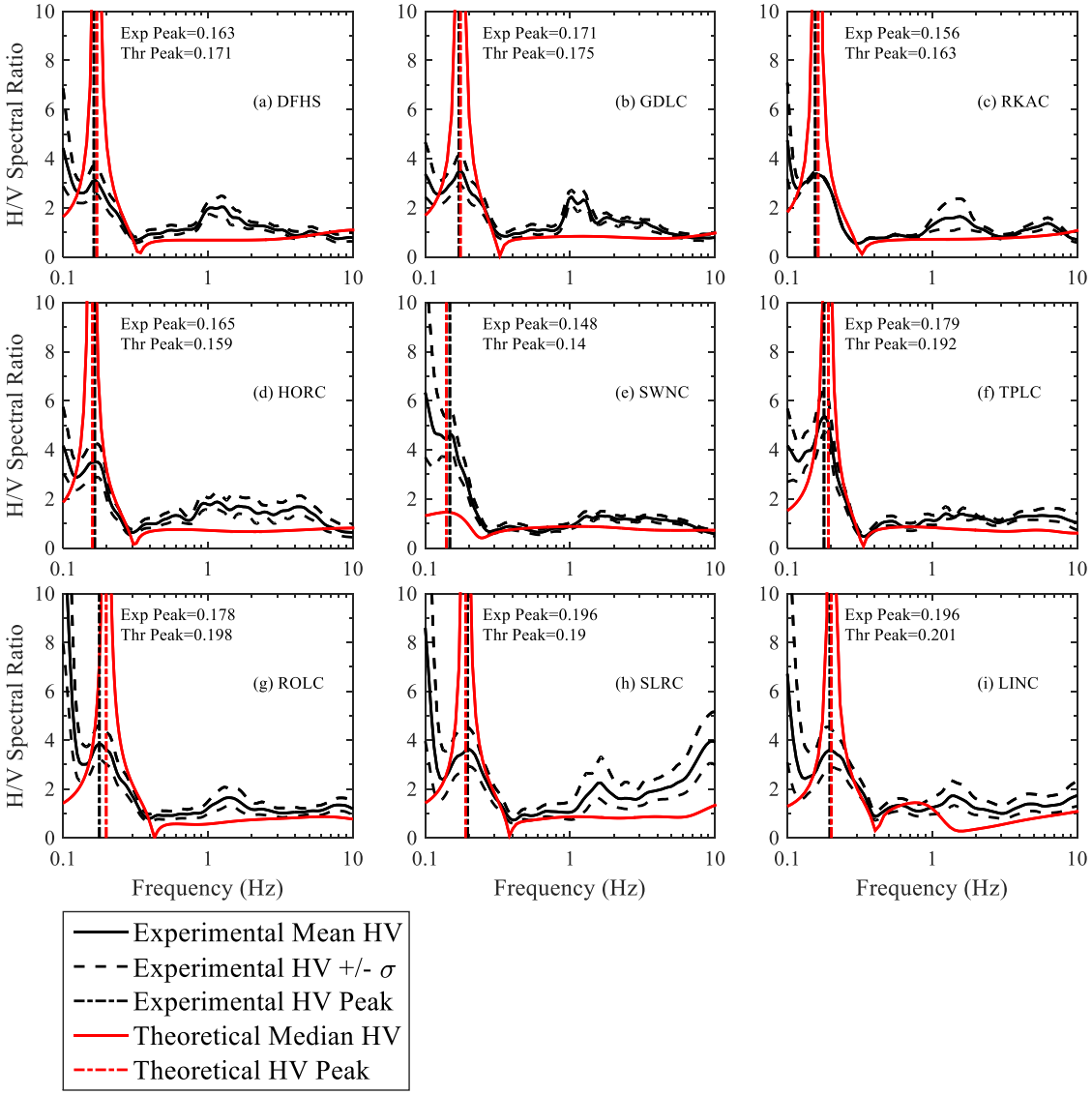

Figure 8. Theoretical HVSR curves generated from the median V_s profile compared to the experimental HVSR curves for each site.

the location of bedrock at each site is characterized by a sharp increase in Vs between 1160-2254 m below the surface. In general, bedrock depths from the inversions were poorly constrained, and typically overestimated or underestimated the location of bedrock at most sites compared to the CVM. This poor constraint is somewhat expected since the bedrock depth at most sites lies beyond the array resolution limits used during testing. However, given the relatively good fits to

the dispersion and HVSR data at each site, the true bedrock depth at each site likely lies within the bedrock estimates from the cloud of Vs profiles from each inversion. This is further supported by the fact that the bedrock depths from the CVM were determined through seismic tomography (Eberhart-Phillips et al. 2010), which has diminished accuracy above three km and seismic reflection lines were sparsely located throughout the Canterbury region (Lee et al. 2017).

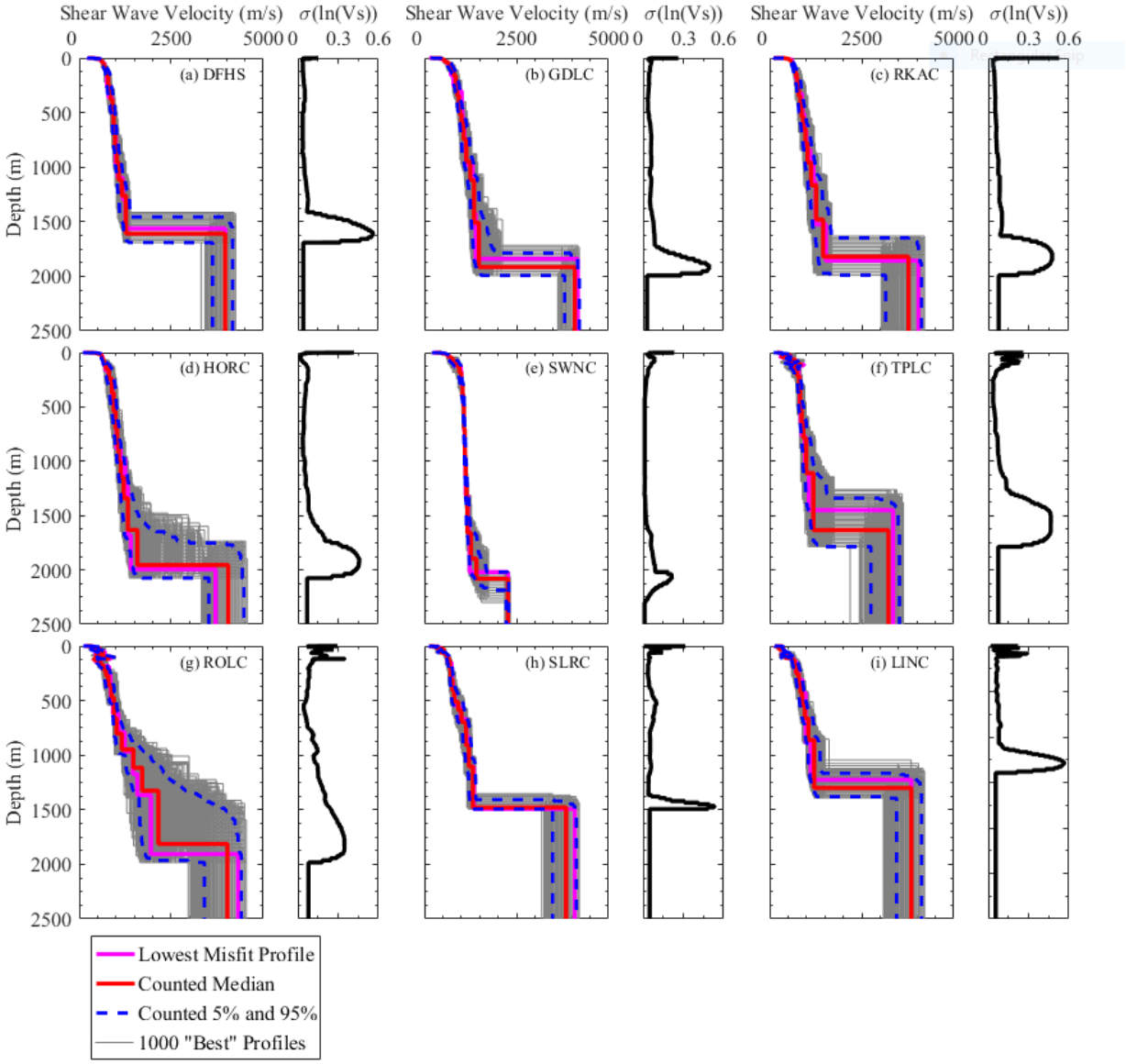

Figure 9. Shear wave velocity profiles resulting from the inversion for each site in this investigation. The shear wave velocity profiles from top 1000 best fit inversion models in gray the median of all 1000 profiles in red. The blue dashed lines represent the counted 5 and 95 percent confidence intervals of the data. Also shown is $\sigma_{(\ln(Vs)}$ in the plot right of the shear wave velocity profiles.

Table 2. Median shear wave velocity (V_s) and depth to layer bottom for each of the nine Canterbury strong motion station sites. The dashed line represents the array resolution limit $k_{min}/2$ (wavenumber/2) Wathelet et al. (2008).

DFHS		GDLC		RKAC		HORC		SWNC		TPLC		ROLC		SLRC		LINC	
V_s (m/s)	Depth (m)	V_s (m/s)	Depth (m)	V_s (m/s)	Depth (m)	V_s (m/s)	Depth (m)	V_s (m/s)	Depth (m)	V_s (m/s)	Depth (m)	V_s (m/s)	Depth (m)	V_s (m/s)	Depth (m)	V_s (m/s)	Depth (m)
278	0	195	0	112	0	180	0	368	0	193	0	205	0	127	0	134	0
382	1.1	247	1.6	357	1.2	347	0.4	427	0.8	273	0.7	310	0.7	257	2.1	229	1.4
426	2.8	452	2.5	452	2.7	440	1.4	457	3.1	322	2.9	353	2.7	329	5.0	343	2.1
541	7.1	490	7.2	510	7.2	485	4.0	541	6.0	347	5.1	394	6.3	382	6.9	356	8.3
580	11	520	11	546	11	557	7.7	586	12	395	10	457	8.8	308	13	371	16
602	19	550	20	573	19	594	12	620	22	549	19	538	15	414	17	232	21
626	32	590	31	596	30	612	28	658	33	327	32	582	25	488	22	270	26
652	42	639	40	614	41	626	45	698	52	467	40	391	33	529	29	389	36
675	54	682	50	636	51	652	58	734	84	567	50	482	38	447	47	412	48
695	73	719	71	651	72	685	77	786	123	699	62	571	44	555	61	476	64
719	90	755	96	677	91	731	106	834	203	507	78	645	55	587	74	314	77
734	101	801	119	704	120	811	152	894	302	658	95	469	74	622	86	558	84
763	119	851	161	733	147	890	240	940	414	844	107	626	89	657	106	411	100
790	169	894	242	759	184	939	372	993	518	658	120	795	103	687	133	620	109
822	252	936	345	793	237	987	540	1034	676	744	145	404	117	715	207	671	127
856	315	967	418	833	349	1032	697	1068	820	801	212	486	127	759	307	727	172
903	381	1007	517	867	427	1074	851	1122	975	829	319	545	140	809	410	787	254
934	460	1063	591	907	536	1129	1004	1191	1215	871	530	610	158	920	512	833	344
972	614	1140	744	972	645	1210	1147	1264	1465	916	647	669	183	1007	590	884	429
1021	797	1246	950	1031	778	1323	1339	1383	1698	992	787	732	221	1129	697	958	541
1073	958	1349	1119	1128	959	1582	1632	1575	1949	1186	1109	793	274	1210	910	1053	662
1162	1119	1480	1509	1264	1166	4050	1955	2102	2274	3224	1634	880	359	1316	1105	1210	861
1271	1261	4084	1916	1453	1480			3803	2625			946	472	3847	1479	3847	1301
3964	1609			3771	1820							1014	661				
												1154	803				
												1474	948				
												1711	1116				
												2152	1326				
												4027	1813				

6. COMPARISON OF V_S PROFILES

Median V_s profiles from each Canterbury SMS tested in this study are compared in Figure 10 along with the median V_s profiles detailed by Teague et al. (2017) at 14 sites in the city of Christchurch. The Canterbury sites, as discussed previously, are separated into two categories: interbedded and gravel only sites. Therefore, with the inclusion of the Teague et al. (2017) profiles, there are three datasets of profiles in Figure 10 (i.e., Canterbury gravel only, Canterbury interbedded, and Christchurch interbedded). As stated earlier, the V_s profiles developed by

Teague et al. (2017) were all measured at sites with interbedded geologic profiles making them similar to the interbedded sites in this study. Because the depth to bedrock across the Canterbury Basin varies so significantly (200-2000 m), the bedrock layers for each V_s profile were grayed out on the plot to make comparison of the sedimentary velocities more straightforward.

Comparing the V_s profiles from the three datasets, the V_s of soil layers above bedrock but deeper than approximately 250 m compare well for the three datasets with sigma ln V_s of approximately 0.07 between all V_s profiles. However, significantly more variability exists for layers shallower than 250 m with an average sigma ln V_s of 0.21 between all V_s profiles. This higher variability in the top 250 m is partially caused by the gravel sites having a consistently higher V_s than the interbedded sites although lower individual variability (sigma ln V_s of 0.04). The second and likely more significant cause of the large variability in the top 250 m is the higher variability in the interbedded V_s profiles in top 250 m (average sigma ln V_s of 0.18), which is likely a result of mixing the V_s of different geologic materials (i.e., mixing the velocity of sand and gravel layers from different V_s profiles). Overall, this indicates all V_s profiles are similar and can be combined below a depth 250 m, but differ and need to be separated above a depth 250 m.

Median V_s profiles are also compared to reference V_s profiles developed by Lin et al. (2014) in Figure 10. Using the reference V_s profiles, the soils in the top 250 m were rudimentarily classified into three groups: very dense gravels, gravels, and soft soils (sand, silt, and clay). Layers classified as soft soil typically correspond to velocity reversals (i.e., sand layers in the CVM) of Canterbury and Christchurch interbedded sites. Layers classified as gravel typically correspond to higher velocity layers (i.e., gravel layers in the CVM) at Canterbury and

Christchurch interbedded sites. Layers classified as very dense gravel typically correspond to layers from the Canterbury gravel only sites.

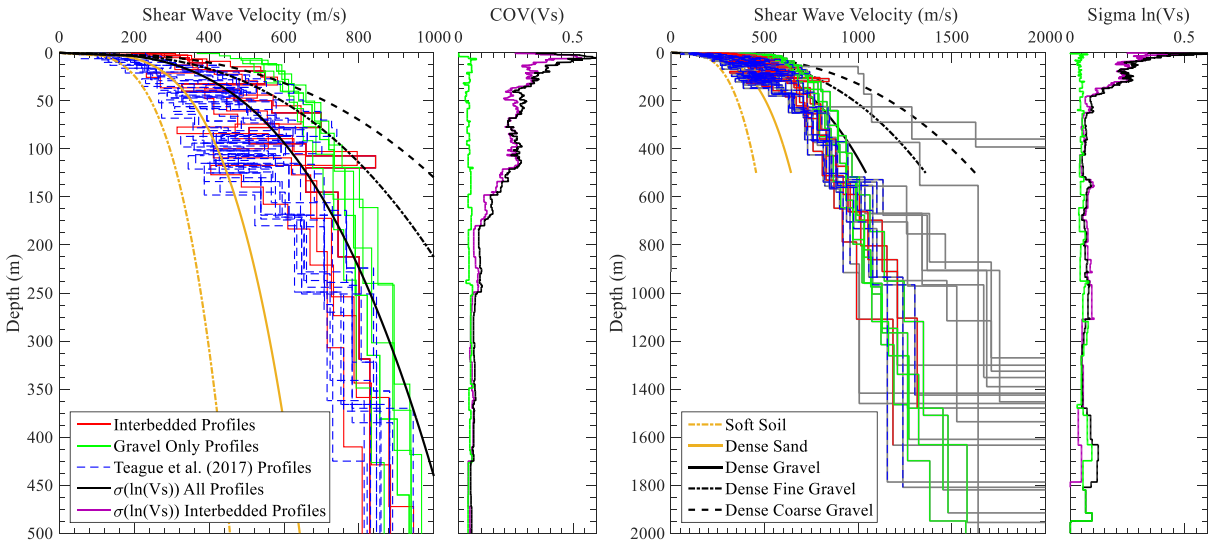

Figure 10. Median V_s profiles from each of the nine sites in this investigation and the 14 Teague et al. (2017) sites. The V_s profiles are complimented by reference velocity profiles (Lin et al. 2014). Along with $\sigma_{ln(Vs)}$ to show uncertainty. The profiles are separated by site type: interbedded sites in the Canterbury plains, gravel only sites in the Canterbury plains, and interbedded sites in Christchurch (Teague et al. 2017). The gray lines represent the bedrock layers of these profiles.

7. DEVELOPMENT OF REFERENCE V_S PROFILES

For layers in each V_s profile, the velocity and median depth for each layer were determined (referred to as center velocity points or CVPs) and plotted in Figure 11. The CVPs were divided into five groups based on (1) soil type (soft soil, gravel or, very dense gravel) from the Lin et al. (2014) reference V_s profiles, (2) site location (interbedded or gravel), and (3) developer (this study or Teague et al. (2017)). These groups are shown in Table 3 along with one additional group, the Canterbury basement gravels (CBG), which includes all CVPs. A first order power-law function, following the format used by Lin et al. (2014), was fit to the CVPs in the top 500 m

for each group. These fits are shown in Figure 11. The power law functional form is provided in Equation 1.

Table 3. Soil groups encountered in the Canterbury basin from this study and the Teague et al. (2017) study.

Soil Group	Acronym
Canterbury Basement Gravels	CBG
Canterbury Interbedded Soft Soils	CISS
Canterbury Interbedded Gravels	CIG
Canterbury Gravel Only	CGO
Teague et al. (2017) Interbedded Soft Soils	TISS
Teague et al. (2017) Interbedded Gravels	TIG

$$V_s = A_s * (\sigma'_o / P_a)^{n_s} \quad \text{Equation 1}$$

Where:

- A_s = shear wave velocity corresponding to one atmosphere mean effective stress
- σ'_o = mean effective stress
- P_a = atmospheric pressure (1 atm)
- n_s = empirical normalized mean effective stress exponent

Based on the power law fits, the TISS and CISS curves (interbedded soft soils) and the TIG and CIG curves (interbedded gravel soils) have very similar coefficients and plot very close to one another indicating good agreement between the interbedded V_s profiles in this study and the Teague et al. (2017) study. In addition, in Figure 11, the sigma ln V_s between the TISS and CISS and TIG and CIG curves are less than 0.092 also indicating good agreement between the corresponding datasets. Therefore, it was determined that the TISS and CISS CVPs could be combined into one dataset and the TIG and CIG CVPs could be combined into one dataset. Since

the velocity of the CGO curve was significantly higher than the interbedded curves, it was not combined with other datasets. Below a depth of approximately 500 m, the sigma ln V_s of the entire data (shown in Figure 11) is less than 0.1 indicating good agreement between all datasets below 500 m. Therefore, it was determined that three reference V_s profiles (interbedded soft soils, interbedded gravels, and gravel only) should be developed in the top 500 m and only one curve (basement gravel) for depths greater than 500 m.

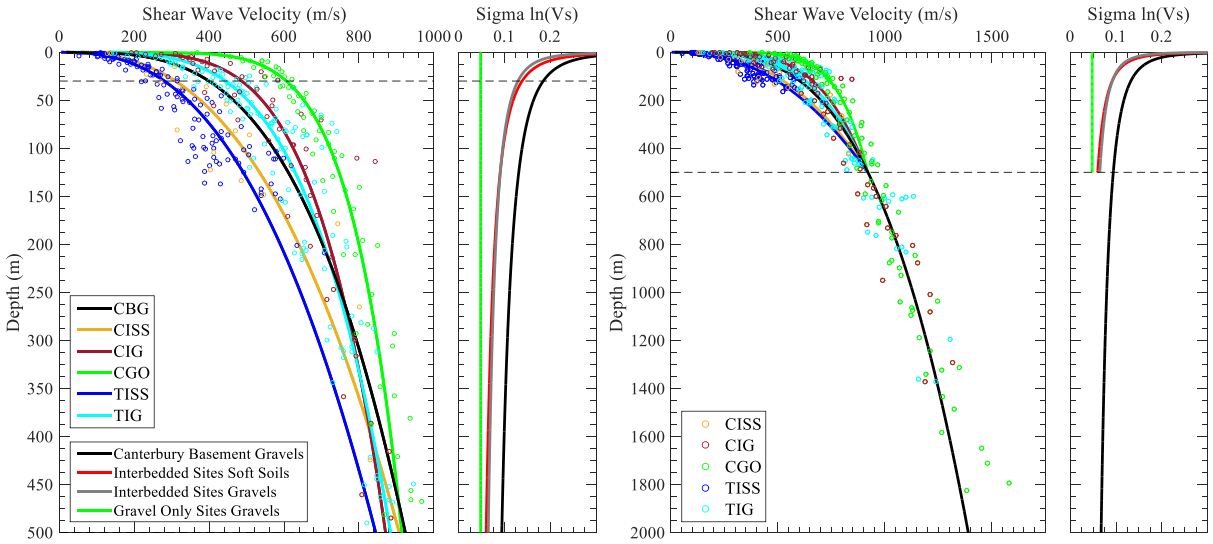

Figure 11. Power fits through the median shear wave velocities of the various soils encountered in the Canterbury plains and sigma ln Vs to estimate uncertainty. The soils are separated into three main categories from both investigations: soft soils or sands, gravels from the interbedded sites, and very stiff gravel from the gravel only sites. Note that CS represents Canterbury Sites and TS represents Teague et al. (2017) sites (Christchurch).

The four, region and soil specific, reference V_s profiles discussed previously are shown in Figure 12 along with the CVPs used to create the profiles. The coefficients used in Equation 1 to create each profile are tabulated in Table 4. To compute σ'_o, a uniform unit weight of 17.3 kN/m^3 for soft soils, 19.6 kN/m^3 for gravels, and 18.8 kN/m^3 for the CBG curve was used. To create continuity between the curves, each curve was constrained through a depth of 500 m and a V_s of 920 m/s. This prevents discontinuities in the curves and does not change the co-efficient

significantly. To estimate the uncertainty of each profile, Equation 2 was fit to the sigma ln V_s computed for each profile where a, b, and c are fitting coefficients and Z is depth below the surface.

$$\sigma_{\ln(V_s)} = a * Z^b - c \qquad \text{Equation 2}$$

At depths greater than 30 m, each reference V_s profile generally has a $\sigma_{\ln(Vs)}$ less than 0.1-0.15. However, at depths less than 30 m, a higher uncertainty ($\sigma_{\ln(Vs)}$) is observed. Therefore, it is not recommended that the reference V_s profiles be used for depths shallower than 30 m. Rather, a shallow site-specific V_s profile should be measured at the site and potentially used with the reference V_s profiles. At 500 m, the dashed line in Figure 12, represents that point where one should start utilizing the CBG reference V_s profile rather than the soil specific reference V_s profiles.

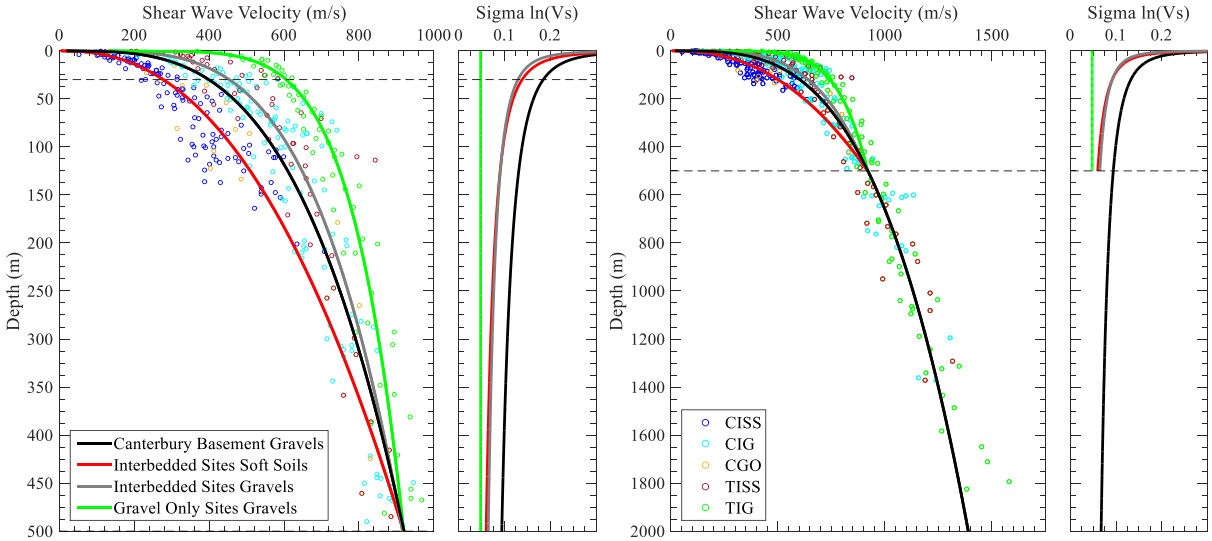

Figure 12. Region and soil specific reference V_s profiles based on each dataset. Sigma ln Vs is shown for each curve to estimate uncertainty.

Table 4. Parameters used in region specific velocity profiles for shear wave velocity and sigma ln V_s estimation.

	V_s		$\sigma_{ln(Vs)}$		
Material	A_s	n_s	a	b	c
Gravel only sites gravels	546.87	0.15	0	0	0.0478*
Interbedded sites gravels	368.88	0.26	0.333	-0.275	0
Interbedded sites soft soils	228.64	0.44	0.448	-0.299	0
Canterbury basement gravels	327.21	0.31	0.415	-0.238	0

*The COV was effectively constant at all depths for the gravel only sites

8. CONCLUSIONS

The V_s structure for the geologically complex Canterbury region of New Zealand was characterized at nine SMS scattered through the region using a combination of active and passive surface wave methods and HVSR. Sites were located on soil deposits between 1100 and 2300 m deep consisting of either stiff gravel or interbedded layers of gravels and softer soils. The interbedded geology tended to produce higher mode Love wave dispersion data over fundamental mode. Furthermore, at each site a zone of complex wave propagation developed between 1 and 10-20 Hz, which made mode assignment more ambiguous. To develop V_s profiles in this geologically complex area, significant a priori geologic information was compiled in an effort to constrain the solution space of the inversion models. The V_s profiles were developed through an iterative multi-mode, multi-method inversion process including Rayleigh and Love wave dispersion data and HVSR peaks. V_s profiles were developed with estimates of associated uncertainty at each site (a maximum of 2300 m). V_s profiles developed in this study were combined with V_s profiles from the 14 Christchurch sites (Teague et al. 2017), to develop a suite of four region and soil specific reference V_s profiles for the Canterbury basin, which may be used to define deep V_s properties across the Canterbury plains. Site specific and reference V_s profiles developed as part of this study can be used for back-analysis of earthquake ground motions,

forward analysis of future ground motions, full 3D physics based simulations, or to refine 3D velocity models for the region.

9. REFERENCES:

Ari, H. and Tokimatsu, K. (2005) S-Wave Velocity Profiling by Joint Inversion of Microtremor Dispersion Curve and Horizontal-to-Vertical (H/V) Spectrum, Bulletin of the Seismological Society of America, 95(5), 1766–1778, DOI: 10.1785/0120040243.

Asten, M. W. and Boore, D. M. (2005) Comparison of shear-velocity profiles of unconsolidated sediments near the Coyote borehole (CCOC) measured with fourteen invasive and non-invasive methods, Blind comparisons of shear-wave velocities at closely-spaced sites in San Jose, California, M. W. Asten and D. M. Boore (Editors), U.S. Geological Survey Open-File Report OFR 2005-1169 (1.0 Mb).

Barnes, P., Castellazzi, C., Gorman, A., and Wilcox, S. (2011) Submarine Faulting Beneath Pegasus Bay. Offshore Christchurch (pp. 46pp): NIWA.

Bettig, B., Bard, P.Y., Scherbaum, F., Riepl, J., Cotton, F., Cornou, C., and Hatzfield, D. "Analysis of dense array noise measurements using the modified spatial auto correlation method (SPAC): application to the Grenoble area." Bollettino de Geofisica Teoria e Applicata, 42(3-4), 281-304.

Bradley B.A. and Graves R.W. (2014) Low frequency (f<1Hz) ground motion simulations of 10 events in the 2010-2011 Canterbury earthquake sequence. Southern California Earthquake Centre (SCEC) Annual Meeting. Palm Springs, California.

Capon, J. (1969) High Resolution Frequency-Wavenumber Spectrum Analysis, Proceedings of IEEE, 57(8), 1408–1418.

Cox, B.R. and Teague, D. (2016) Layering Ratios: A Systematic Approach to the Inversion of Surface Wave Data in the Absence of A-priori Information, Geophysical Journal International, 207, 422–438.

Cox, B.R. and Wood, C.M. (2011) Surface Wave Benchmarking Exercise: Methodologies, Results and Uncertainties, Proc. GeoRisk 2011, Atlanta, GA, June 26-28.

Cox, B.R., Wood. C.M., and Teague, D.P. (2014) Synthesis of the UTexas1 Surface Wave Dataset Blind-Analysis Study: Inter-Analyst Dispersion and Shear Wave Velocity Uncertainty. Geo-Congress 2014 Technical Papers: Geo-Characterization and Modeling for Sustainability. GSP 234.

Cubrinovski, M., Bradley, B.A., Wotherspoon, L., Green, R., Bray, J., Wood, C., Pender, M., Allen, J., Bradshaw, A., Rix, G., Taylor, M., Robinson, K., Henderson, D., Giorgini, S., Ma, K., Winkley, A., Zupan, J. (2011) Geotechnical Aspects of the 22 February 2011 Christchurch earthquake, Bulletin of the New Zealand Society of Earthquake Engineering, Special Issue on the 22 February 2011 Christchurch earthquake, 2011, Vol 44 No 4, pp 181-194.

DiGiulio, G., Savvaidis, A., Ohrnberger, M., Wathelet, M., Cornou, C., Knapmeyer-Endrun, B., Renalier, F., Theodoulidis, N. and Bard, P.Y. (2012) Exploring the model space and ranking a best class of models in surface-wave dispersion inversion: Application at European strong-motion sites, Geophysics, 77(3), B147–B166.

Dunkin, J.W. (1965) Computation of modal solutions in layered, elastic media at high frequencies, Bulletin of the Seismological Society of America, 55, 335–358.

Eberhart-Phillips, D. (2010) Establishing a versatile 3-D seismic velocity model for New Zealand. Seismological Research Letters, 81(6), 992-1000.

Forsyth, P.J., Barrell, D.J.A., Jongens, R. (2008) Geology of the Christchurch area, Lower Hutt, New Zealand, GNS Science.

Green, R.A., Cubrinovski, M., Bradley, B., Henderson, D., Kailey, P., Robinson, K., Taylor, M., Winkley, A., Wotherspoon, L., Orense, R., Pender, M., Hogan, L., Allen, J., Bradshaw, A., Bray, J., DePascale, G., O'Rourke, T., Rix, G., Wells, D., and Wood, C. (2012) Geotechnical Aspects of the Mw 6.2 2011 Christchurch, New Zealand, Earthquake, GeoCongress 2012: State of the Art and Practice in Geotechnical Engineering . GSP 225. 2012.

Haskell, N. A. (1953) The dispersion of surface waves on multilayered media, Bulletin of Seismological Society of America, 43, 17–34.

Knopoff L. (1964) A matrix method for elastic wave problems. Bulletin of Seismological Society of America, 54, 431–438.

Konno, K. and Ohmachi, T. (1998) Ground-motion characteristics estimated from spectral ratio between horizontal and vertical components of microtremor, Bulletin of the Seismological Society of America, 88, 228-241.

Lee, R.L., Bradley, B.A., Ghisetti, F.C., Pettinga, J.R., Hughes, M.W. and Thomson, E.M. (2015) A geology-based 3D seismic velocity model of Canterbury, New Zealand, in Proceedings of the 2015 NZSEE Conference, Paper O-63, 570-577.

Lee, R., Bradley, B., and McGann, C. (2017) 3D Models for the Interbedded Quaternary Stratigraphy in the Canterbury, New Zealand Region, New Zealand Journal of Geology and Geophysics, in press.

Lin, Y.C., Joh, S.H, and Stokoe, K. H. (2014) Analyst J: Analysis of the UTexas 1 Surface Wave Dataset Using the SASW Methodology, Geo-Congress 2014 Technical Papers: Geo-Characterization and Modeling for Sustainability. GSP 234. 2014.

Park, C.B., Miller, R.D. & Xia, J. (1999) Multichannel analysis of surface waves, Geophysics, 64: 800-880.

Parolai, S., Picozzi, M., Richwalski, S.M., and Milkereit, C. (2005) Joint Inversion of phase velocity dispersion and H/V ratio curves from seismic noise recordings using a genetic algorithm, considering higher modes, Geophysical Research Letters, 32(1), L01303, DOI: 10.1029/2004GL021115.

Rosenblad, B.L. and Goetz, R. (2010) Study of the H/V spectral ratio method for determining average shear wave velocities in the Mississippi embayment, Engineering Geology, Volume 112, Issue 1, 2010, Pages 13-20.

Scherbaum, F., Hinzen, K.G., and Ohrnberger, M. (2003) Determination of shallow shear wave velocity profiles in the Cologne/Germany area using ambient vibrations. Geophysical Journal International 152, 597–612.

SESAME European project (2004) Guidelines for the Implementation of the H/V Spectral Ratio Technique on Ambient Vibrations: Measurements, Processing and Interpretation. Deliverable D23.12.

Taylor ML., Cubrinovski M. and Bradley BA. (2012) Characterisation of ground conditions in the Christchurch central business District. Australian Geomechanics Journal 47(4): 43-57.

Teague, D., Cox, B., Bradley, B. and Wotherspoon, L.M. (2017) Development of Deep Shear Wave Velocity Profiles with Estimates of Uncertainty in the Complex Inter-Bedded Geology of Christchurch, UNKNOWN JOURNAL...

Teague, D., Cox, B., Bradley, B. and Wotherspoon, L.M. (2015) Development of Realistic Vs Profiles in Christchurch, New Zealand via Active and Ambient Surface Wave Data: Methodologies for Inversion in Complex Interbedded Geology, in Proceedings of the 6th International Conference on Earthquake Geotechnical Engineering, Christchurch, NZ, 1–4. November 2015.

Teague, D., Cox, B., Bradley, B. and Wotherspoon, L.M. (2017) Development of Deep Shear Wave Velocity Profiles with Estimates of Uncertainty in the Complex Inter-Bedded Geology of Christchurch, in review.

Thomson, W. T. (1950) Transmission of elastic waves through a stratified solid medium, Journal of Applied Physics, 21, 89–93.

Wathelet, M., Jongmans, D., and Ohrnberger, M. (2004) Surface-wave inversion using a direct search algorithm and its application to ambient vibration measurements, Near Surface Geophysics, 2(4).

Wathelet, M. (2008). An improved neighborhood algorithm: parameter conditions and dynamic scaling. Geophysical Research Letters, 35, L09301, doi:10.1029/2008GL033256.

Wood, C.M., Cox, B.R., Wotherspoon, L.M. & Green, R.A. (2011) Dynamic site characterization of Christchurch strong motion stations, Bulletin of the NZSEE, 44(4): 195-204.

Wood. C., Ellis, T., Teague, D., & Cox, B. (2014) Analyst I: Comprehensive Analysis of the UTexas1 Surface Wave Dataset, ASCE Geo-Congress 2014: Geo-Characterization and Modeling for Sustainability, Atlanta, GA, 23-26 February 2014.

Wotherspoon, L.M., Bradley, B.A., Hills, A., Thomson, E.M., Jeong, S., Wood, C.M., Cox, B.R. (2015) Development of deep VS profiles and site periods for the Canterbury region, New Zealand Society for Earthquake Engineering Conference. 10-12 April 2015. Rotorua, New Zealand.

Wotherspoon, L.M., Orense, R.P., Bradley, B.A., Cox, B.R., Wood, C.M. & Green, R.A. (2014) Geotechnical characterisation of Christchurch strong motion stations, Earthquake Commission Biennial Grant Report, Project No. 12/629, 2013.

Zywicki, D.J. (1999). Advanced signal processing methods applied to engineering analysis of seismic surface waves. Ph.D. Dissertation, School of Civil and Environmental Engineering, Georgia Institute of Technology, Atlanta, GA, p. 357.